

Field propagation in de Sitter black holes

C. Molina, D. Giugno^y and E. Abdalla^z
Instituto de Física, Universidade de São Paulo
C.P. 66318, 05315-970, São Paulo-SP, Brazil

A. Saa^x
Departamento de Matemática Aplicada, UNICAMP
C.P. 6065, 13083-859, Campinas-SP, Brazil

We present an exhaustive analysis of scalar, electromagnetic and gravitational perturbations in the background of Schwarzschild-de Sitter and Reissner-Nordström-de Sitter spacetimes. The field propagation is considered by means of a semi-analytical (WKB) approach and two numerical schemes: the characteristic and general initial value integrations. The results are compared near the extreme cosmological constant regime, where analytical results are presented. A unifying picture is established for the dynamics of different spin fields.

PACS numbers: 04.30.Nk, 04.70.Bw

I. INTRODUCTION

Wave propagation around non-trivial solutions of Einstein equations, black holes in particular, is an active field of research (see [1, 2, 3] and references therein). The perspective of gravitational waves detection in a near future and the great development of numerical general relativity have increased even further the activity on this field. Gravitational waves should be especially strong when emitted by black holes. The study of the propagation of perturbations around them is, hence, essential to provide templates for the gravitational waves identification. On the other hand, recent astrophysical observations indicate that the universe is undergoing an accelerated expansion phase, suggesting the existence of a small positive cosmological constant and that de Sitter (dS) geometry provides a good description of very large scales of the universe [4]. We notice also that string theory has recently motivated many works on asymptotically anti-de Sitter spacetimes (see, for instance, [5, 6, 7, 8]).

In this work, we perform an exhaustive investigation of scalar, electromagnetic and gravitational perturbations in the background of Schwarzschild-de Sitter (SdS) and Reissner-Nordström-de Sitter (RNdS) spacetimes. Contrasting with the non-charged case, in the RNdS one the electromagnetic and gravitational perturbations are necessarily coupled. We scan the full range of the cosmological constant, from the asymptotic flat case ($\Lambda = 0$) up to the critical value of Λ which characterizes, for the non-charged case, the Nariai solution [9]. Two different numerical methods and a higher order WKB analysis are used. The results are compared near the extreme regime, where analytical results can be obtained.

We remind that for any perturbation in the spacetimes we consider, after the initial transient phase there are two main contributions to the resulting asymptotic wave [10, 11]: initially the so-called quasinormal modes, which are suppressed at later time by the tails. The first can be understood as candidates to normal modes which, however, decay (their energy eigenvalues becomes complex), as in the ingenious mechanism first described by G. Gamow in the context of nuclear physics [12]. After the initial transient phase, the properties of resulting wave are more related to background spacetime rather than to the source itself.

It is well known that for asymptotically flat backgrounds the tails decay according to a power-law, whereas in a space with a positive cosmological constant the decay is exponential. Curiously, $\Lambda = 0$ modes for scalar fields in dS spacetimes, contrasting to the asymptotic flat cases, approach exponentially a non-vanishing asymptotic value [13, 14]. We detected, by using a non-characteristic numerical integration scheme, a dependence of this asymptotic value on the initial velocities. In particular, it vanishes for static initial conditions. Our results are in perfect agreement with the analytical predictions of [14].

The semi-analytical analyses of this work were performed by using the higher order WKB method proposed by Schutz and Will [15], and improved by Iyer and Will [16, 17]. It provides a very accurate and systematic way to study black hole quasinormal modes. We apply it to the study of various perturbation fields in the non-asymptotically flat dS geometry. Quasinormal modes are also calculated according to this approximation, and the results are compared to the numerical ones whenever appropriate, providing a quite complete picture of the question of quasinormal perturbations for dS black holes.

Concerning the charged case, we analyze in detail the wave propagation of the massless scalar field and coupled electromagnetic and gravitational fields in the RNdS spacetime. An important difference concerning the dynamics of the electromagnetic and gravitational fields is

^Electronic address: cmolina@fma.ifusp.br

^yElectronic address: dgiugno@fma.ifusp.br

^zElectronic address: eabdalla@fma.ifusp.br

^xElectronic address: asaa@in.eun.unicamp.br

that there are no pure modes, since both are inter-related. We will show that the direct picture of the evolution presents us with a perfect agreement on quasinormal frequencies with those obtained by using the approximation method suggested in [15, 16]. One important point assessed is the dependence of the fields' decay on the electric charge of the black hole, including the asymptotically at limit, for which we expected to find traces of a power-law tail appearing between the quasinormal modes and the exponential tail.

Two very recent works overlap our analysis presented here. A similar WKB approach, presented in [18], was used very recently by Zhidenko [19] to study SdS black holes, giving results in agreement with ours. Yoshida and Futamase [20] used a continued fraction numerical code to calculate quasinormal mode frequencies, with special emphasis to high order modes. Our results are also compatible. Finally, we notice that solutions of the wave equation in a non-trivial background have also been used to infer intrinsic properties of the spacetime [21].

The paper is organized as follows: section II provides theoretical considerations and reviews some well-known results which were useful to our work; section III briefly explains the numerical and semi-analytical methods employed, followed by section IV, which presents, in detail, our results on field dynamics for near extreme SdS and RNdS geometries. Section V deals with the so-called intermediate region, where the geometries are not extreme. Data on the SdS limit and on exponential tails are also presented. Section VI deals with the near asymptotically at region and section VII presents our conclusions.

II. METRIC, FIELDS AND EFFECTIVE POTENTIALS

The metric describing a charged, asymptotically de Sitter spherical black hole, written in spherical coordinates, is given by

$$ds^2 = -h(r)dt^2 + h(r)^{-1}dr^2 + r^2(d\theta^2 + \sin^2\theta d\phi^2); \quad (1)$$

where the function $h(r)$ is

$$h(r) = 1 - \frac{2m}{r} + \frac{q^2}{r^2} - \frac{r^2}{3} : \quad (2)$$

The integration constants m and q are the black hole mass and electric charge respectively. If the cosmological constant is positive, we have the Reissner-Nordstrom-de Sitter metric. In this case, h is usually written as $h = 3/a^2$, where the constant a is the "cosmological radius".

The spacetime causal structure depends strongly on the zeros of $h(r)$. Depending on the parameters m , q and a , the function $h(r)$ may have three, two, or even no real positive zeros. For the RNdS cases we are interested, $h(r)$ has three simple real, positive roots (r_c , r_+ and r_-), and a real and negative root $r_n = -(r + r_+ + r_c)$. The horizons r_- , r_+ and r_c , with $r_- < r_+ < r_c$, are denoted Cauchy, event and cosmological horizons respectively.

For the SdS case ($q = 0$), and assuming $m > 0$ and $0 < 9m^2 < 1$, the function $h(r)$ has two positive zeros r_+ and r_c and a negative zero $r_n = -(r_+ + r_c)$. This is the SdS geometry in which we are interested. The horizons r_+ and r_c , with $r_+ < r_c$, are denoted event and cosmological horizons respectively. In this case, the constants m and a are related with the roots by

$$a^2 = r_+^2 + r_c^2 + r_+ r_c; \quad (3)$$

$$2ma^2 = r_+ r_c (r_+ + r_c) : \quad (4)$$

If $9m^2 = 1$, the zeros r_+ and r_c degenerate in a double root. This is the extreme SdS black hole. If $9m^2 > 1$, there is no real positive zeros, and the metric (1) does not describe a black hole.

In both SdS and RNdS cases, we shall study the perturbation fields in the exterior region, defined as

$$T_+ = f(t; r; \ell, m); r_+ < r < r_c : \quad (5)$$

In this region T_+ , we define a "tortoise coordinate" $x(r)$ in the usual way,

$$x(r) = \frac{1}{2} \frac{1}{r_c} \ln(r_c - r) + \frac{1}{2} \frac{1}{r_+} \ln(r - r_+) - \frac{1}{2} \frac{1}{r_n} \ln(r - r_n) + \frac{1}{2} \frac{1}{r_n} \ln(r - r_n); \quad (6)$$

with

$$\ell = \frac{1}{2} \frac{dh(r)}{dr} \Big|_{r=r_i} : \quad (7)$$

The constants r_c , r_+ and r_n are the surface gravities associated with the Cauchy, event and cosmological horizons respectively. For the SdS case, the term associated with the Cauchy horizon is absent.

Consider now a scalar perturbation field obeying the massless Klein-Gordon equation

$$\square \phi = 0 : \quad (8)$$

The usual separation of variables in terms of a radial field and a spherical harmonic $Y_{\ell m}(\theta, \phi)$,

$$\phi = \sum_{\ell, m} \frac{1}{r} \psi_{\ell m}(t; r) Y_{\ell m}(\theta, \phi); \quad (9)$$

leads to Schrodinger-type equations in the tortoise coordinate for each value of ℓ ,

$$\frac{\partial^2 \psi_{\ell m}}{\partial t^2} + \frac{\partial^2 \psi_{\ell m}}{\partial x^2} = V^{\ell m}(x) \psi_{\ell m}; \quad (10)$$

where the effective potential $V^{\ell m}$ is given by

$$V^{\ell m}(x) = h(r) \left[\frac{\ell(\ell+1)}{r^2} + \frac{2m}{r^3} - \frac{2q^2}{r^4} - \frac{2}{a^2} \right] : \quad (11)$$

The situation for higher spin perturbations is quite different. In the SdS geometry, in contrast to the case of an electrically charged black hole, it is possible to have pure electromagnetic and gravitational perturbations. For both cases, we have Schrodinger-type effective equations. For the first, the effective potential is given [22]

$$V^{\text{el}}(r) = h(r) \frac{(\ell' + 1)}{r^2}; \quad (12)$$

with $\ell' = 1$. The gravitational perturbation theory for the exterior Schwarzschild-de Sitter geometry has been developed in [2, 5]. The potentials for the axial and polar modes are, respectively,

$$V^{\text{ax}}(r) = h(r) \frac{(\ell' + 1)}{r^2} - \frac{6m}{r^3}; \quad (13)$$

$$V^{\text{po}}(r) = \frac{2h(r)}{r^3 (3m + cr)^2} [9m^3 + 3c^2 m r^2 + c^2 (1 + c) r^3 + 3m^2 (3cr - r^3)]; \quad (14)$$

with $2c = (\ell' - 1)(\ell' + 2)$ and $\ell' = 2$. For perturbations with $\ell' > 0$, we can show explicitly that all the effective potentials $V(x) = V(r(x))$ are positive definite. For scalar perturbations with $\ell' = 0$, however, the effective potential has one zero point x_0 and it is negative for $x > x_0$.

The perturbation theory for the RNdS geometry has been developed in [23]. There are neither purely electromagnetic nor gravitational modes. Indeed, we have four mixed electromagnetic and gravitational fields, two of them called polar fields, Z_1^+ and Z_2^+ (since they impart no rotation to the black hole) and two named axial fields, Z_1^- and Z_2^- . It is possible to express their dynamics in four decoupled wave equations, two for the axial fields and two for the polar fields. Their deduction can be found in [23] and references therein. Here we just show the expressions which will be useful throughout our work.

The axial perturbations $Z_{1,2}$ are governed by wave equations which have the same form of (10), but with effective potentials given by

$$V_1 = h(r) \left[\frac{(\ell' + 1)}{r^2} + \frac{4q^2}{r^2} - \frac{3m}{r^3} \sqrt{\frac{9m^2 + 8\alpha q^2}{9m^2 + 8\alpha q^2}} \right]; \quad (15)$$

$$V_2 = h(r) \left[\frac{(\ell' + 1)}{r^2} + \frac{4q^2}{r^2} - \frac{3m}{r^3} \sqrt{\frac{9m^2 + 8\alpha q^2}{9m^2 + 8\alpha q^2}} \right]; \quad (16)$$

respectively, with $2c = (\ell' - 1)(\ell' + 2)$.

The polar perturbations $Z_{1,2}^+$ are subjected to rather cumbersome potentials, as we can see below:

$$V_1^+ = \frac{h(r)}{r^3} U + \frac{1}{2} (p_1 - p_2) W; \quad (17)$$

$$V_2^+ = \frac{h(r)}{r^3} U - \frac{1}{2} (p_1 - p_2) W; \quad (18)$$

$$p_1 = 3m + \sqrt{\frac{9m^2 + 8\alpha q^2}{9m^2 + 8\alpha q^2}}; \quad (19)$$

$$p_2 = 3m - \sqrt{\frac{9m^2 + 8\alpha q^2}{9m^2 + 8\alpha q^2}}; \quad (20)$$

$$W = \frac{rh(r)}{r^{1/2}} (2cr + 3m) + \frac{1}{r^{1/2}} (cr + m) + \frac{2}{3} r^3; \quad (21)$$

$$U = (2cr + 3m)W + \frac{1}{r^{1/2}} (cr - m) + \frac{2}{3} r^3 - \frac{2cr^2 h(r)}{r^{1/2}}; \quad (22)$$

$$r = cr + 3m - \frac{2q^2}{r}; \quad (23)$$

In the limit $q \rightarrow 0$, the RNdS potentials V_2 go into the SdS polar and axial potentials, V^\pm . Therefore, the minimum ℓ' for these fields is $\ell' = 2$, while the V_1 fields admit $\ell' = 1$ as their minimum ℓ' -value, since they become electromagnetic perturbations in the limit $q \rightarrow 0$.

III. NUMERICAL AND SEMI-ANALYTICAL APPROACHES

A. Characteristic integration

In the work [24] a simple but at the same time very efficient way of dealing with two-dimensional differential equations has been set up. Along the general lines of the pioneering work [25], the authors introduced light-cone variables $u = t - x$ and $v = t + x$, in terms of which all the wave equations introduced have the same form. We call V the generic effective potential and ψ the generic field, and the equations can be written, in terms of the null coordinates, as

$$4 \frac{\partial^2}{\partial u \partial v} \psi(u; v) = V(r(u; v)) \psi(u; v); \quad (24)$$

In the characteristic initial value problem, initial data are specified on the two null surfaces $u = u_0$ and $v = v_0$. Since the basic aspects of the field decay are independent of the initial conditions (this fact is confirmed by our simulations), we use

$$\psi(u = u_0; v) = \exp \left[\frac{(v - v_0)^2}{2} \right]; \quad (25)$$

$$\psi(u; v = v_0) = \exp \frac{(v_0 - v_c)^2}{2 \sigma^2} ; \quad (26)$$

Due the size of our lattices, the latter constant can be set to zero for any practical purpose.

Since we do not have analytic solutions to the time-dependent wave equation with the effective potentials introduced, one approach is to discretize the equation (24), and then implement a finite differencing scheme to solve it numerically. One possible discretization, used for example in [8, 13, 14], is

$$\psi(N) = \psi(W) + \psi(E) - \psi(S) \\ + 2V(S) \frac{\psi(W) + \psi(E)}{8} + O(\Delta^4); \quad (27)$$

where we have used the definitions for the points: $N = (u + \Delta u; v + \Delta v)$, $W = (u + \Delta u; v)$, $E = (u; v + \Delta v)$ and $S = (u; v)$. With the use of expression (27), the basic algorithm will cover the region of interest in the $u-v$ plane, using the value of the field at three points in order to compute it at a fourth.

After the integration is completed, the values $\psi(u_{max}; v)$ and $\psi(u; v_{max})$ are extracted, where u_{max} (v_{max}) is the maximum value of u (v) on the numerical grid. Taking sufficiently large u_{max} and v_{max} , we have good approximations for the wave function at the event and cosmological horizons.

B. Non-characteristic integration

It is not difficult to set up a numeric algorithm to solve equation (10) with Cauchy data specified on a t constant surface. We used 4th order in x and 2nd in t scheme (see, for instance, [26] for an application of this algorithm to seismic analysis). The second spatial derivative at a point $(t; x)$, up to 4th order, is given by

$$\psi''(t; x) = \frac{1}{12 \Delta x^2} [\psi(t; x + 2 \Delta x) - 16 \psi(t; x + \Delta x) \\ + 30 \psi(t; x) - 16 \psi(t; x - \Delta x) \\ + \psi(t; x - 2 \Delta x)]; \quad (28)$$

while the second time derivative up to 2nd order is

$$\psi''(t; x) = \frac{\psi(t + \Delta t; x) - 2 \psi(t; x) + \psi(t - \Delta t; x)}{\Delta t^2} ; \quad (29)$$

Given $\psi(t = t_0; x)$ and $\psi'(t = t_0 - \Delta t; x)$ (or $-\psi'(t = t_0; x)$), we can use (28) and (29) discretization to solve (10) and calculate $\psi(t = t_0 + \Delta t; x)$. This is the basic algorithm. At each interaction, one can control the error by using the invariant integral (the wave energy) associate to (10)

$$E = \frac{1}{2} \int_{-\infty}^{\infty} (\psi'(t; x))^2 + (\psi''(t; x))^2 + V(x) \psi(t; x)^2 dx ; \quad (30)$$

We make exhaustive analysis of the asymptotic behavior of the solutions of (10) with initial conditions of the form

$$\psi(0; x) = \exp \frac{(x - x_0)^2}{2 \sigma_0^2} ; \quad (31)$$

$$-\psi(0; x) = A \exp \frac{(x - x_1)^2}{2 \sigma_1^2} ; \quad (32)$$

The results do not depend on the details of initial conditions. They are compatible with the ones obtained by the usual characteristic integration, with the only, and significative, exception of the $\psi = 0$ scalar mode. As we will see, its asymptotic value depends strongly on the initial velocities $-\psi(0; x)$, a behavior already advanced in the work [14].

C. WKB analysis

Considering the Laplace transform of the equation (10), one gets the ordinary differential equation

$$\frac{d^2 \psi(x)}{dx^2} - (s^2 + V(x)) \psi(x) = 0 ; \quad (33)$$

One finds that there is a discrete set of possible values to s such that the function $\hat{\psi}$, the Laplace-transformed field, satisfies both boundary conditions,

$$\lim_{x \rightarrow 1} \hat{\psi} e^{sx} = 1 ; \quad (34)$$

$$\lim_{x \rightarrow -1} \hat{\psi} e^{-sx} = 1 ; \quad (35)$$

By making the formal replacement $s = i\omega$, we have the usual quasinormal mode boundary conditions. The frequencies ω (or s) are called quasinormal frequencies.

The semi-analytic approach used in this work [15, 16] is a very efficient algorithm to calculate the quasinormal frequencies, which have been applied in a variety of situations [17]. With this method, the quasinormal modes are given by

$$\omega_n^2 = (V_0 + P) \left(i n + \frac{1}{2} \right)^2 - 2V_0^{(2)} \frac{1}{2} (1 + Q) \quad (36)$$

where the quantities P and Q are determined using

$$P = \frac{1}{8} \frac{V_0^{(4)}}{V_0^{(2)}} - \frac{1}{4} + \frac{1}{288} \frac{V_0^{(3)}}{V_0^{(2)}}^2 + 60 \sigma^2 ; \quad (37)$$

(38)

$$n = \begin{pmatrix} 0; 1; 2; \dots & \text{Re}(!_n) > 0; \\ 1; 2; 3; \dots & \text{Re}(!_n) < 0; \end{pmatrix} \quad (39)$$

$$= \frac{r_c}{r_+} r_+ ; \quad (43)$$

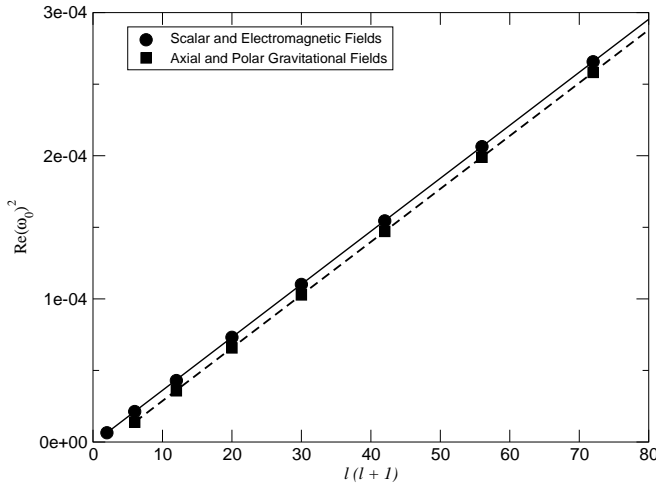


Figure 2: Curve of $\text{Re}(\omega_0)^2$ with $\ell(\ell+1)$, for the scalar, electromagnetic and gravitational fields, in the near extremal limit. The dots are the numerical results and the solid lines represent the analytical results. The parameters for the geometry are $m = 1.0$ and $a = 0.01$.

where $0 < \ell < 1$. In this limit the dynamics can be analytically characterized, as has been analyzed in [27]. More general settings, including RN dS geometries, were explored in [28].

The function $h(x) = h(r(x))$ can be analytically calculated [27, 28], with the result

$$h(x) = \frac{(r_c - r_+)}{2 \cosh^2(x + x_0)} + O(x^{-3}) : \quad (44)$$

We have ve different fields at hand: scalar field (Z_{sc}), two axial fields (Z_1, Z_2) and two polar fields (Z_1^+, Z_2^+). For each one, we have a different potential. In the near

extremal limit, we have

$$V(x) = (r_+ - r_c)h(x) + O(x^{-3}) = \frac{V_0}{\cosh^2(x + x_0)} + O(x^{-3}) : \quad (45)$$

The constant V_0 in the scalar case is denoted by V_0^{sc} , in the axial cases by $fV_0^1; V_0^2$ and in the polar cases by $fV_0^{1+}; V_0^{2+}$. The foregoing expression is a Pöschl-Teller potential [29].

For the scalar field, V_0^{sc} has been calculated in [28], being given by

$$V_0^{sc} = \frac{\ell(\ell+1)(r_c - r_+)}{2r_+^2} : \quad (46)$$

We proceed to the analysis of the coupled electromagnetic and gravitational fields. We take the analytical expressions for all potentials $V_{1,2}$ and we go to the near extremal limit. For the two axial potentials, we have

$$V_0^1 = \frac{(r_c - r_+)}{2r_+^4} \ell(\ell+1)r_+^2 + 4q^2 - S_1 : \quad (47)$$

$$V_0^2 = \frac{(r_c - r_+)}{2r_+^4} \ell(\ell+1)r_+^2 + 4q^2 - S_2 : \quad (48)$$

where

$$S_1 = 3m \sqrt{\frac{p}{9m^2 + 4(\ell+2)(\ell-1)q^2}} : \quad (49)$$

$$S_2 = 3m + \sqrt{\frac{p}{9m^2 + 4(\ell+2)(\ell-1)q^2}} : \quad (50)$$

We can now turn to the two polar potentials. The constants V_0^{1+} and V_0^{2+} are given by

$$V_0^{1+} = \frac{(r_c - r_+)}{2r_+^4} \left[\frac{2}{4} \frac{2cr_+^2 + 3m r_+ + r_+^p \sqrt{\frac{p}{9m^2 + 8cq^2}}}{cr_+ + 3m \frac{2q^2}{r_+}} + C \frac{7}{5} \right] : \quad (51)$$

$$V_0^{2+} = \frac{(r_c - r_+)}{2r_+^4} \left[\frac{2}{4} \frac{2cr_+^2 + 3m r_+ + r_+^p \sqrt{\frac{p}{9m^2 + 8cq^2}}}{cr_+ + 3m \frac{2q^2}{r_+}} + C \frac{7}{5} \right] : \quad (52)$$

with $C = 2m r_+ - 2q^2 \frac{2}{3} \frac{r_+^4}{3}$ and $2c = (\ell+2)(\ell-1)$. The quasinormal modes associated with the Pöschl-Teller potential have been extensively studied [30, 31]. The

frequencies ω_n are given by

$$\omega_n = \frac{V_0}{2} \frac{1}{4} i n + \frac{1}{2} : \quad (53)$$

with $n = 0, 1, 2, \dots$ labeling the modes. Using expression (53) and the expression for V_0 , the frequencies can be

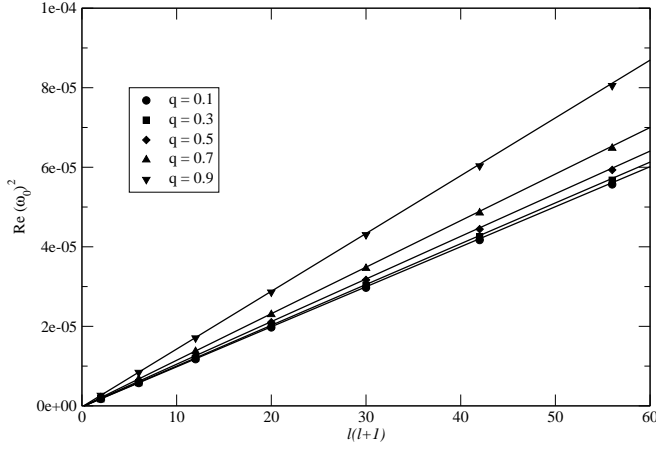


Figure 3: Near extremal fundamental frequencies for different values of the charge q , for the lower multipole mode of the scalar field. Analytical values are represented by straight lines, and numerical values appear as dots. The parameters for the geometry are $m = 1.0$ and $\Lambda = 10^{-3}$.

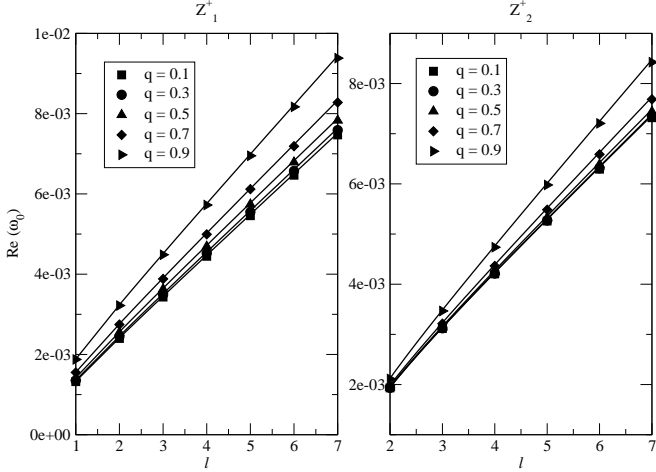


Figure 4: Near extremal fundamental frequencies for different values of the charge q , for the lower multipole mode of the polar fields. On the left are the data for Z_1^+ and, on the right, for Z_2^+ . The parameters for the geometry are $m = 1.0$ and $\Lambda = 10^{-3}$.

easily calculated.

We can also use the numerical method to analyze the field decay in the near extremal limit. Using a non-linear fitting based in χ^2 analysis for the wave functions, we can estimate the quasinormal frequencies. These results can be compared with the analytical expressions in the near extremal cases. The accordance between both sets of results is extremely good. We illustrate this point in figures 3 to 5.

Direct calculation of the wave functions confirms that, in the near extremal limit, the dynamics of the fields is simple, with a late time decay being completely dominated by quasinormal modes.

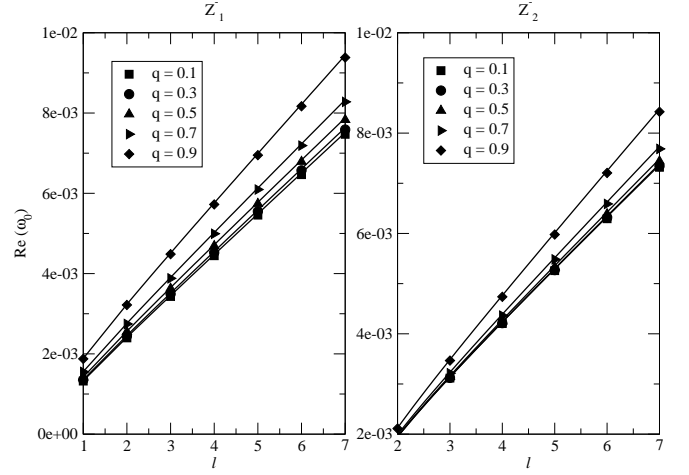


Figure 5: Near extremal fundamental frequencies for different values of the charge q , for the lower multipole mode of the axial fields. The data for Z_1^- appear on the left, and those for Z_2^- , on the right. The parameters for the geometry are $m = 1.0$ and $\Lambda = 10^{-3}$.

V. INTERMEDIATE REGION IN PARAMETER SPACE

A. Schwarzschild-de Sitter black hole

1. Scalar Field with $\ell = 0$

Only scalar perturbations can have zero total angular momentum. Solutions of (10) with $\ell = 0$ leads to a constant tail, as already shown in [13, 14]. This is confirmed in figure 6. The novelty here is the dependence of the asymptotic value on the $-\langle 0|x\rangle$ initial condition. Figure 6 reveals the appearance of the constant value ϕ_0 for large t , and its dependence on $-\langle 0|x\rangle$. Note that ϕ_0 falls below 10^{-7} for $-\langle 0|x\rangle = 0$. These results are in accordance with the analytical predictions of [14], which give

$$\langle 1|r\rangle = \frac{r}{r_c^2} \int_0^{r_c} -\langle 0;s\rangle s \frac{ds}{h^0(s)} : \quad (54)$$

2. Fields with $\ell > 0$

We can have scalar and vector fields with angular momentum $\ell = 1$, and with $\ell > 1$, it is possible to introduce also gravitational fields. Their behavior is described in general by three phases. The first corresponds to the quasinormal modes generated from the presence of the black hole itself. A little later there is a region of power-law decay, which continues indefinitely in an asymptotic at space. In the presence of a positive cosmological constant, however, an exponential decay takes over in the latest period.

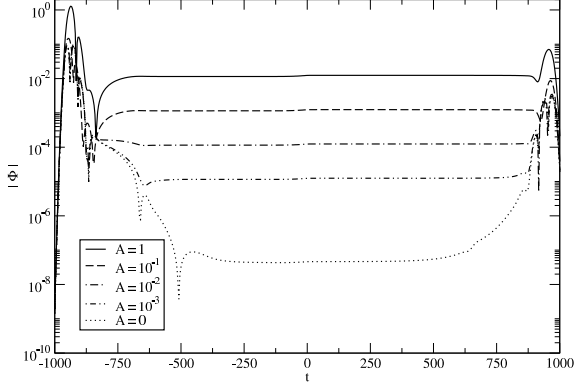


Figure 6: Asymptotic solutions $|\Phi|$ obtained by non-characteristic numerical integration with $\ell = 0$, $\kappa_+ = 10^{-4}$ and $m = 1.0$. The curves correspond to different values of A in the initial condition (32).

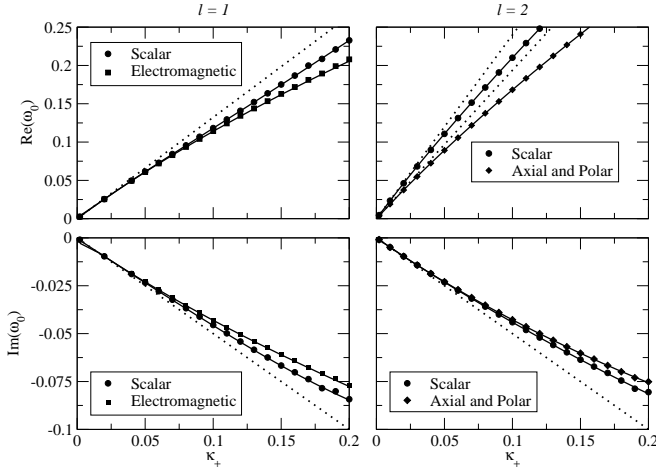


Figure 7: Graphs of the real and imaginary part of the fundamental frequencies ($n = 0$) with κ_+ . The dotted lines are the near extreme results, the dots are the numerical results and the continuous curves are the semi-analytic results. In the graphs, $m = 1.0$.

As the separation of the horizons increases, the quasinormal frequencies deviate from those predicted by expressions (41) and (42). In Figure 7, this is illustrated for $\ell = 1, 2$. Some qualitatively different effects show up when we turn away from the near extreme limit. For a small cosmological constant the asymptotic behavior is dominated by an exponentially decaying mode rather than by a quasinormal mode, for all perturbations considered.

It is interesting to compare the values obtained for the fundamental modes using the numerical and semi-analytic methods. We find that the agreement between them is good, for the whole range of κ_+ . The difference is smaller for the first values of ℓ . This is expected, since

$q = 0$		Numerical		Semi-analytical	
ℓ		$\text{Re}(\omega_0)$	$-\text{Im}(\omega_0)$	$\text{Re}(\omega_0)$	$-\text{Im}(\omega_0)$
1	1.000E-5	2.930E-01	9.753E-01	2.911E-01	9.780E-02
	1.000E-4	2.928E-01	9.764E-02	2.910E-01	9.797E-02
	1.000E-3	2.914E-01	9.726E-02	2.896E-01	9.771E-02
	1.000E-2	2.770E-01	9.455E-02	2.753E-01	9.490E-02
	1.000E-1	8.159E-02	3.123E-02	8.144E-02	3.137E-02
2	1.000E-5	4.840E-01	9.653E-02	4.832E-01	9.680E-02
	1.000E-4	4.833E-01	8.948E-02	4.830E-01	9.677E-02
	1.000E-3	4.816E-01	8.998E-02	4.809E-01	9.643E-02
	1.000E-2	4.598E-01	8.880E-02	4.592E-01	9.290E-02
	1.000E-1	1.466E-01	3.068E-02	1.466E-01	3.070E-02
3	1.000E-5	6.769E-01	8.662E-02	6.752E-01	9.651E-02
	1.000E-4	6.754E-01	8.654E-02	6.749E-01	9.647E-02
	1.000E-3	6.732E-01	8.660E-02	6.720E-01	9.611E-02
	1.000E-2	6.437E-02	9.200E-02	6.428E-02	9.235E-02
	1.000E-1	2.091E-02	3.054E-02	2.091E-02	3.056E-02

Table I: Fundamental frequencies for the scalar field in SdS, obtained using the numerical and semi-analytical methods. In this table, $m = 1.0$.

the numerical calculations work better in this region. In the table I, we illustrate these observations with a few values of κ_+ . It is important to mention that quasinormal frequencies for the SdS black hole were already calculated in a recent paper [19], applying a variation of the WKB method used here [18]. There are earlier papers calculating quasinormal modes in this geometry, for example [32].

The first higher n modes cannot be obtained from the numerical solution, but can be calculated by the semi-analytic method. As the cosmological constant decreases, the real and imaginary parts of the frequencies increase, up to the limit where the geometry is asymptotically flat. The behavior of the m modes is illustrated in Figure 8. The behavior of the electromagnetic field is similar.

A χ^2 analysis of the data presented in Figure 9 shows that the massless scalar, electromagnetic and gravitational perturbations in SdS geometry behave as

$$\psi^{sc} \sim e^{k_{\text{exp}}^{sc} t} \text{ with } t \rightarrow 1 \quad (55)$$

$$\psi^{el} \sim e^{k_{\text{exp}}^{el} t} \text{ with } t \rightarrow 1 \quad (56)$$

$$\psi^{ax} \sim e^{k_{\text{exp}}^{ax} t} \text{ with } t \rightarrow 1 \quad (57)$$

$$\psi^{po} \sim e^{k_{\text{exp}}^{po} t} \text{ with } t \rightarrow 1 \quad (58)$$

for t sufficiently large. At the event and the cosmological horizons t is substituted, respectively by v and u .

ℓ	$q = 0$	Numerical		Semi-analytical	
		$\text{Re}(\omega_0)$	$-\text{Im}(\omega_0)$	$\text{Re}(\omega_0)$	$-\text{Im}(\omega_0)$
1	1.000E-5	2.481E-01	9.226E-02	2.459E-01	9.310E-02
	1.000E-4	2.481E-01	9.223E-02	2.457E-01	9.307E-02
	1.000E-3	2.475E-01	9.176E-02	2.448E-01	9.270E-02
	1.000E-2	2.374E-01	8.839E-02	2.352E-01	8.896E-02
	1.000E-1	8.035E-02	3.027E-02	8.023E-02	3.033E-02
2	1.000E-5	4.577E-01	8.985E-02	4.571E-01	9.506E-02
	1.000E-4	4.575E-01	8.991E-02	4.569E-01	9.502E-02
	1.000E-3	4.559E-01	9.439E-02	4.551E-01	9.464E-02
	1.000E-2	4.371E-01	8.941E-02	4.364E-01	9.074E-02
	1.000E-1	1.458E-01	3.037E-02	1.458E-01	3.038E-02
3	1.000E-5	6.578E-01	8.365E-02	6.567E-01	9.563E-02
	1.000E-4	6.576E-01	8.349E-02	6.564E-01	9.559E-02
	1.000E-3	6.547E-01	8.399E-02	6.538E-01	9.520E-02
	1.000E-2	6.276E-02	8.852E-02	6.267E-01	9.125E-02
	1.000E-1	2.085E-02	3.039E-03	2.085E-01	3.040E-02

Table II: Fundamental frequencies for the electromagnetic field in SdS, obtained using the numerical and semi-analytical methods. In this table, $m = 1.0$.

ℓ	$q = 0$	Numerical		Semi-analytical	
		$\text{Re}(\omega_0)$	$-\text{Im}(\omega_0)$	$\text{Re}(\omega_0)$	$-\text{Im}(\omega_0)$
2	1.000E-5	3.738E-01	8.883E-02	3.731E-01	8.921E-02
	1.000E-4	3.737E-01	8.880E-02	3.730E-01	8.918E-02
	1.000E-3	3.721E-01	8.850E-02	3.715E-01	8.888E-02
	1.000E-2	3.566E-01	8.538E-02	3.560E-01	8.572E-02
	1.000E-1	1.179E-01	3.020E-02	1.179E-01	3.023E-02
3	1.000E-5	5.999E-01	8.677E-02	5.992E-01	9.272E-02
	1.000E-4	5.996E-01	8.676E-02	5.990E-01	9.269E-02
	1.000E-3	5.972E-01	8.971E-02	5.966E-01	9.234E-02
	1.000E-2	5.725E-01	8.695E-02	5.718E-01	8.874E-02
	1.000E-1	1.900E-01	3.030E-02	1.900E-02	3.032E-02
4	1.000E-5	8.106E-01	8.810E-02	8.091E-01	9.417E-02
	1.000E-4	8.102E-01	8.781E-02	8.087E-01	9.413E-02
	1.000E-3	8.070E-01	8.799E-02	8.055E-01	9.376E-02
	1.000E-2	7.733E-02	8.714E-02	7.720E-01	9.000E-02
	1.000E-1	2.564E-02	3.034E-03	2.563E-01	3.036E-02

Table III: Fundamental frequencies for the axial and polar gravitational fields in SdS, obtained using the numerical and semi-analytical methods. In this table, $m = 1.0$.

The numerical simulations developed in the present work reveal an interesting transition between oscillatory modes and exponentially decaying modes. As shown in figure 10, as the cosmological constant increases, the absolute value of $-\text{Im}(\omega_0)$ decreases.

Above a certain critical value of Λ we do not observe the exponential tail, since the coefficient k_{exp} is larger

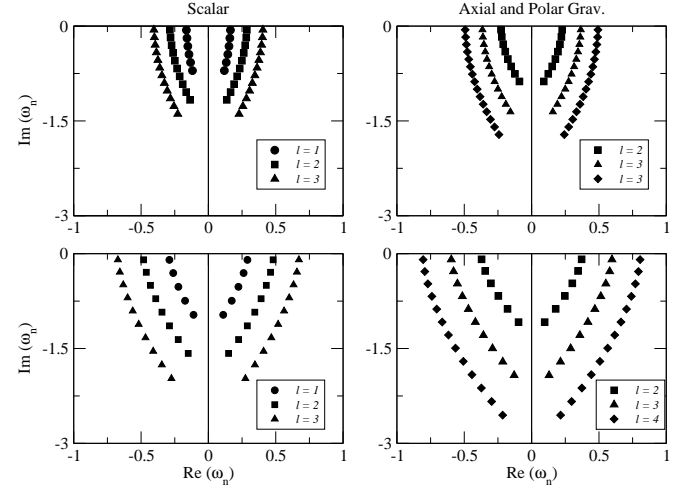


Figure 8: Quasinormal modes of the scalar, axial and polar gravitational fields, for higher m modes. The parameter for the curves are $m = 1.0$ and $\Lambda = 10^{-3}$.

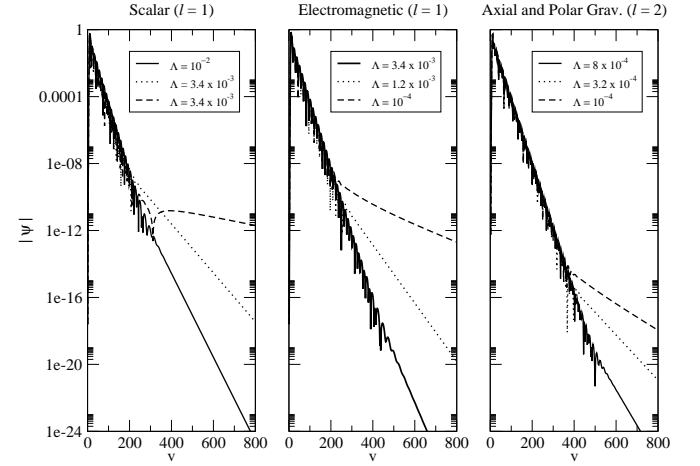


Figure 9: Exponential tail for the scalar and electromagnetic fields with $\ell = 1$, and for the axial and polar gravitational field with $\ell = 2$. In the graphs, $m = 1.0$.

than $-\text{Im}(\omega_0)$ thus the decaying quasinormal mode dominates. But for smaller than this critical value, $-\text{Im}(\omega_0)$ turns out to be larger than k_{exp} and the exponential tail dominates. Certainly, for a small enough cosmological constant the exponential tail dominates in the various cases considered here.

Another aspect worth mentioning in the intermediate region is the dependence of the parameters $k_{\text{exp}}^{\text{sc}}$, $k_{\text{exp}}^{\text{el}}$, $k_{\text{exp}}^{\text{ax}}$ and $k_{\text{exp}}^{\text{po}}$ with Λ and c . The results suggest that the k_{exp} are at least second differentiable functions of c . Therefore, close to $c = 0$, we approximate

$$k_{\text{exp}}^{\text{sc}}(c) = \Lambda_c + c^{\frac{2}{c}}; \quad (59)$$

$$k_{\text{exp}}^{\text{el}}(c) = k_{\text{exp}}^{\text{ax}}(c) = k_{\text{exp}}^{\text{po}}(c) = (\ell + 1) \Lambda_c + c^{\frac{2}{c}}; \quad (60)$$

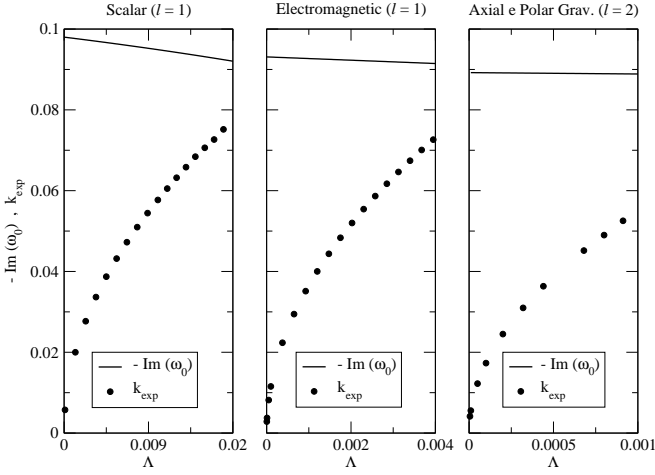


Figure 10: Approaching of the constants $-\text{Im}(\omega_0)$ and k_{exp} , for the scalar, electromagnetic and gravitational fields, in the SdS geometry. Above a certain critical value of Λ (roughly $1.7 \cdot 10^2$, $4.0 \cdot 10^3$ and $1.2 \cdot 10^3$ respectively, for the parameters taken in graphs), a tail it is not observed. For all curves, the mass is set to $m = 1.0$.

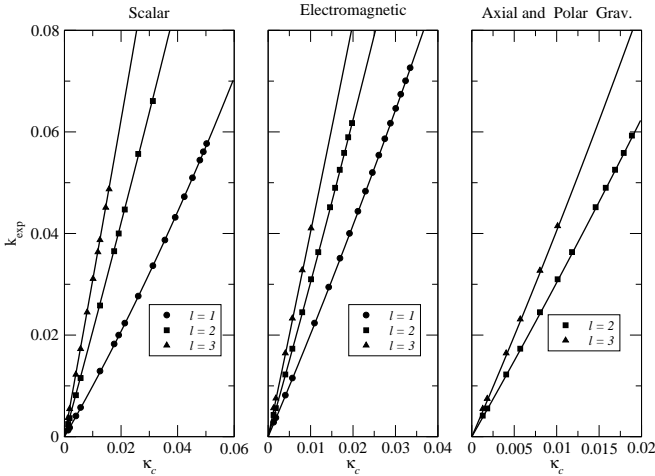


Figure 11: Dependence of k_{exp} with c and l , in the SdS geometry. The symbols indicate the numerical values, and the solid lines are the appropriate fittings. For the left graph: $k_{\text{exp}}^{\text{sc}} = 1.077 \cdot 10^4 + 0.984 c + 3.545 \frac{c^2}{c}$, $k_{\text{exp}}^{\text{sc}} = 1.863 \cdot 10^4 + 2.010 c + 2.608 \frac{c^2}{c}$ and $k_{\text{exp}}^{\text{sc}} = 1.959 \cdot 10^4 + 3.028 c + 2.978 \frac{c^2}{c}$. For the center graph: $k_{\text{exp}}^{\text{el}} = 2.082 \cdot 10^4 + 1.988 c + 6.141 \frac{c^2}{c}$, $k_{\text{exp}}^{\text{el}} = 2.712 \cdot 10^4 + 2.974 c + 8.284 \frac{c^2}{c}$ and $k_{\text{exp}}^{\text{el}} = 3.737 \cdot 10^4 + 3.984 c + 4.517 \frac{c^2}{c}$. For the right graph: $k_{\text{exp}}^{\text{ax}} = 2.616 \cdot 10^4 + 2.974 c + 9.895 \frac{c^2}{c}$ and $k_{\text{exp}}^{\text{ax}} = 4.484 \cdot 10^4 + 3.896 c + 18.92 \frac{c^2}{c}$. In the graphs, $m = 1.0$.

Previous results are illustrated in figure 11.

B. Reissner-Nordstrom-de Sitter black hole

We assess here the behavior of the fields in RNdS exterior geometries which are not near extreme, nor close

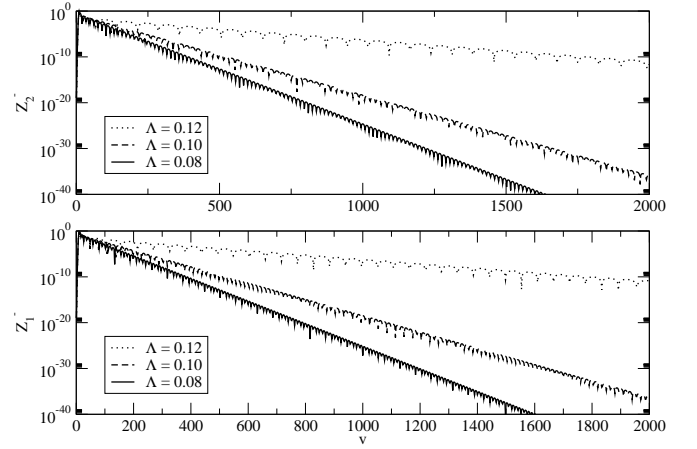


Figure 12: Quasinormal modes for RNdS Z_1 and Z_2 fields. The parameters for the geometry are $q = 0.5$ and $m = 1.0$. We have used $\ell = 2$. The results are similar for the other fields considered.

to the asymptotically flat limit. Direct numerical simulations and semi-analytical (WKB) methods were largely employed to characterize the fields in this region.

For scalar perturbations with $\ell = 0$, the effective potential is not positive definite. As already shown in [13, 14], solutions of (10) with $\ell = 0$ leads to a constant tail. It was observed that in the SdS geometry there is a dependence of the asymptotic value on the $\lim_{x \rightarrow 0} \psi(x)$ initial condition, in the context of a Cauchy type initial value problem. We have checked that the introduction of electric charge does not alter this picture.

If $\ell > 0$, we introduce the Z_1 fields, and for $\ell > 1$ the Z_2 fields can also be analyzed. The first point studied is the quasinormal phase. If the cosmological constant is high enough, the decay is dominated by quasinormal modes, even when they no longer are accurately predicted by the expressions (53). This scenario, illustrated in figure 12, is valid for all fields considered, with any charge smaller than its critical value.

We have observed that the influence of the electric charge is mild, although not trivial. The range of variation of the quasinormal modes with the charge is not very large. We illustrate this point in the figure 13. It is interesting to compare the values obtained for the fundamental modes using the numerical and semi-analytical methods. We find a very good agreement between these results. The difference is smaller for the first values of ℓ . This is expected, since the numerical calculations work better in this region. In the tables IV-V II, we illustrate these observations for a few values of q and Λ .

For all fields considered, with a small enough cosmological constant, there is a qualitative change in the behavior of all fields considered. The late-time decay is dominated by an exponential tail. Therefore in the RNdS geometry we have

$$\psi \sim e^{k_{\text{exp}}^{\text{sc}} t} \text{ with } t \gg 1; \quad (61)$$

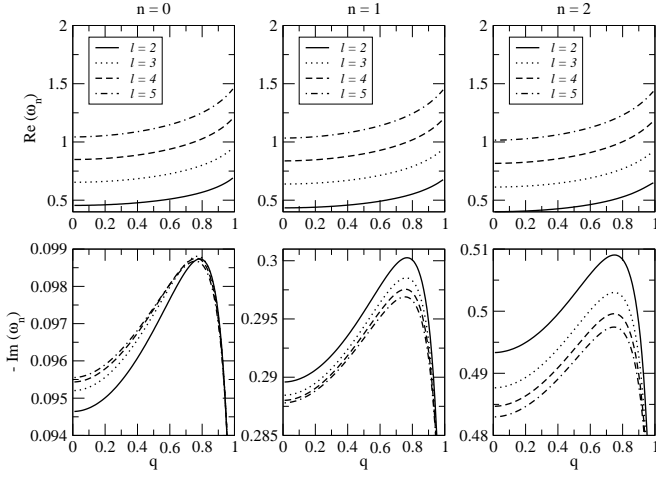


Figure 13: Dependence of Z_1^+ field frequencies on q , for both the real and imaginary parts, in RN dS. The results are qualitatively similar for the other fields considered. The parameters are $m = 1.0$ and $\alpha = 10^{-4}$.

$q = 0.5$		Numerical		Semi-analytical	
ℓ		$\text{Re}(\omega_\ell)$	$-\text{Im}(\omega_\ell)$	$\text{Re}(\omega_\ell)$	$-\text{Im}(\omega_\ell)$
1	1.000E-5	2.71E-1	9.51E-2	3.28E-1	9.53E-2
	1.000E-4	2.71E-1	9.50E-2	3.28E-1	9.53E-2
	1.000E-3	2.70E-1	9.47E-2	3.27E-1	9.49E-2
	1.000E-2	2.60E-1	9.11E-2	3.15E-1	9.14E-2
	1.000E-1	1.16E-1	4.08E-2	1.40E-1	4.08E-2
2	1.000E-5	4.94E-1	9.72E-2	4.94E-1	9.71E-2
	1.000E-4	4.93E-1	9.72E-2	4.94E-1	9.71E-2
	1.000E-3	4.91E-1	9.68E-2	4.92E-1	9.67E-2
	1.000E-2	4.73E-1	9.31E-2	4.73E-1	9.30E-2
	1.000E-1	2.09E-1	4.10E-2	2.09E-1	4.16E-2
3	1.000E-5	7.05E-1	8.95E-2	7.05E-1	9.77E-2
	1.000E-4	7.05E-1	8.94E-2	7.05E-1	9.76E-2
	1.000E-3	7.02E-1	8.87E-2	7.02E-1	9.73E-2
	1.000E-2	6.77E-1	8.50E-2	6.76E-1	9.35E-2
	1.000E-1	2.98E-1	4.10E-2	2.98E-1	4.10E-2

Table IV: Fundamental frequencies for the Z_1 field in RN dS, with $q = 0.5$ and $m = 1.0$, using the numerical and semi-analytical methods.

$$Z_1 = e^{k_{\text{exp}}^1 t} \text{ with } t \gg 1; \quad (62)$$

$$Z_2 = e^{k_{\text{exp}}^2 t} \text{ with } t \gg 1; \quad (63)$$

for t sufficiently large. At the event and the cosmological horizons t is substituted by v and u respectively. Figure 14 illustrates this point, which has been noticed by [13, 14] for scalar fields, and we have extended this consideration to the coupled electromagnetic and gravitational fields. In the aforementioned figure we compare

$q = 0.5$		Numerical		Semi-analytical	
ℓ		$\text{Re}(\omega_\ell)$	$-\text{Im}(\omega_\ell)$	$\text{Re}(\omega_\ell)$	$-\text{Im}(\omega_\ell)$
2	1.000E-5	3.82E-1	8.96E-2	3.81E-1	8.98E-2
	1.000E-4	3.82E-1	8.96E-2	3.81E-1	8.98E-2
	1.000E-3	3.80E-1	8.93E-2	3.80E-1	8.95E-2
	1.000E-2	3.66E-1	8.67E-2	3.65E-1	8.67E-2
	1.000E-1	1.60E-1	4.06E-2	1.60E-1	4.05E-2
3	1.000E-5	6.13E-1	8.59E-2	6.12E-1	9.33E-2
	1.000E-4	6.13E-1	8.59E-2	6.12E-1	9.32E-2
	1.000E-3	6.10E-1	8.59E-2	6.10E-1	9.29E-2
	1.000E-2	5.88E-1	8.50E-2	5.87E-1	8.97E-2
	1.000E-1	2.58E-1	4.07E-2	2.59E-1	4.07E-2

Table V: Fundamental frequencies for the Z_2 field in RN dS, with $q = 0.5$ and $m = 1.0$, using the numerical and semi-analytical methods.

$q = 0.5$		Numerical		Semi-analytical	
ℓ		$\text{Re}(\omega_\ell)$	$-\text{Im}(\omega_\ell)$	$\text{Re}(\omega_\ell)$	$-\text{Im}(\omega_\ell)$
1	1.000E-5	2.71E-1	9.51E-2	2.69E-1	9.55E-2
	1.000E-4	2.71E-1	9.50E-2	2.68E-1	9.55E-2
	1.000E-3	2.70E-1	9.47E-2	2.67E-1	9.51E-2
	1.000E-2	2.60E-1	9.11E-2	2.57E-1	9.15E-2
	1.000E-1	1.16E-1	4.08E-2	1.16E-1	4.08E-2
2	1.000E-5	4.94E-1	9.71E-2	4.93E-1	9.72E-2
	1.000E-4	4.94E-1	9.71E-2	4.93E-1	9.72E-2
	1.000E-3	4.92E-1	9.67E-2	4.91E-1	9.68E-2
	1.000E-2	4.73E-1	9.30E-2	4.73E-1	9.31E-2
	1.000E-1	2.09E-1	4.16E-2	2.09E-1	4.10E-2
3	1.000E-5	7.05E-1	8.95E-2	7.05E-1	9.77E-2
	1.000E-4	7.05E-1	8.94E-2	7.05E-1	9.76E-2
	1.000E-3	7.02E-1	8.86E-2	7.02E-1	9.73E-2
	1.000E-2	6.77E-1	8.50E-2	6.76E-1	9.35E-2
	1.000E-1	2.98E-1	4.10E-2	2.98E-1	4.10E-2

Table VI: Fundamental frequencies for the Z_1 field in RN dS, with $q = 0.5$ and $m = 1.0$, using the numerical and semi-analytical methods.

the exponential tails at the event horizon for exterior RN dS geometries.

An important point is that, unlike the QNM frequencies, the exponential coefficients have shown no dependence on the black hole's electric charge, for all kinds of fields at hand. Close to $\alpha_c = 0$, our results are compatible with the expressions

$$k_{\text{exp}}^{\text{sc}}(\alpha_c) = \ell(\ell+1)\alpha_c + \alpha_c^{\text{sc}} \frac{\alpha_c^2}{\alpha_c}; \quad (64)$$

$$k_{\text{exp}}^{\text{t}}(\alpha_c) = (\ell+1)\alpha_c + \alpha_c^{\text{t}} \frac{\alpha_c^2}{\alpha_c} \quad i=1,2; \quad (65)$$

$q = 0.5$		Numerical		Semi-analytical	
ℓ		$\text{Re}(\omega_\ell)$	$-\text{Im}(\omega_\ell)$	$\text{Re}(\omega_\ell)$	$-\text{Im}(\omega_\ell)$
2	1.000E-5	3.82E-1	8.96E-2	3.81E-1	8.99E-2
	1.000E-4	3.82E-1	8.95E-2	3.81E-1	8.97E-2
	1.000E-3	3.80E-1	8.93E-2	3.79E-1	8.94E-2
	1.000E-2	3.66E-1	8.64E-2	3.65E-1	8.66E-2
	1.000E-1	1.60E-1	4.13E-2	1.60E-1	4.05E-2
3	1.000E-5	6.13E-1	8.56E-2	6.12E-1	9.33E-2
	1.000E-4	6.13E-1	8.56E-2	6.12E-1	9.32E-2
	1.000E-3	6.10E-1	8.56E-2	6.10E-1	9.29E-2
	1.000E-2	5.88E-1	8.49E-2	5.87E-1	8.97E-2
	1.000E-1	2.58E-1	4.07E-2	2.58E-1	4.07E-2

Table V II: Fundamental frequencies for the Z_2^+ eld in RN dS, with $q = 0.5$ and $m = 1.0$, using the numerical and semi-analytical methods.

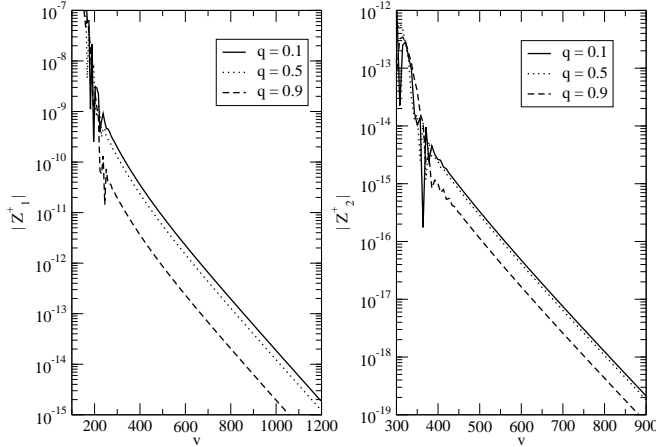


Figure 14: Tails of the Z_1^+ ($\ell = 1$) and Z_2^+ ($\ell = 2$) elds in RN dS. The parameters for the geometry are $\Lambda = 10^{-4}$ and $m = 1.0$. The results are similar for the other elds considered.

for any q lower than its extreme value. The dynamics of the elds in de Sitter spacetimes is therefore much different from the similar cases in anti-de Sitter geometries, in which for high charge there is an abrupt change in the elds' decay [8]. We have also explicitly assessed the behavior of the $Z_{1,2}$ elds as $q \rightarrow 0$, comparing their quasinormal frequencies and exponential tails to those observed in the SdS Z_ℓ elds. As anticipated, we found that the Z_2^+ eld behaves as the SdS Z_2^+ eld and that the Z_2^- eld behaves as the SdS Z_2^- eld, if the charge is small enough. We have observed that the RN dS elds Z_2 tend smoothly to the SdS elds Z_2 .

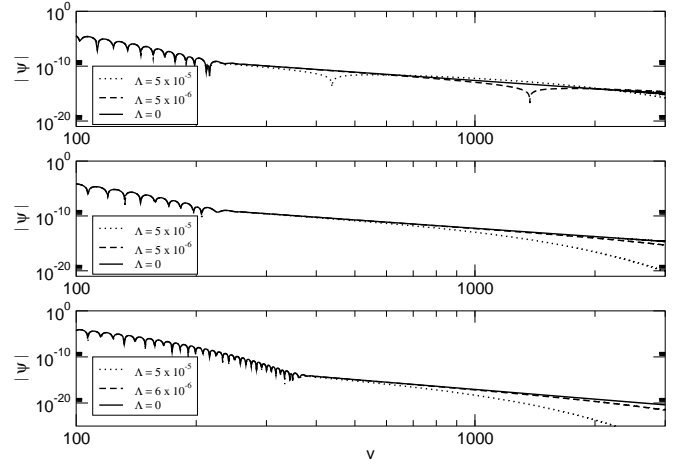


Figure 15: Approaching the asymptotically flat geometry in SdS. Straight lines in the log-log graphs indicate power-law decay. In the graphs, $m = 1.0$.

VI. APPROACHING THE ASYMPTOTICALLY FLAT GEOMETRY

Scalar elds in the SdS geometry near the asymptotically flat limit were studied in [13, 14]. In this case there is a clear separation between the event and the cosmological horizons, such that

$$\frac{r_c}{r_+} \ll 50 : \quad (66)$$

A new qualitative change occurs in this regime, namely a decaying phase with a power-law behavior. Such a phase occurs between the quasinormal mode decay and the exponential decay phases. The eld cannot be simply described by a superposition of the various modes, which would imply a domination of the power-law phase. This is illustrated in figure 15.

The situation for RN dS cases obeying (66) is presented in figure 16. As can be seen in this figure, we have a perfect power-law tail developing for large v when $\Lambda = 0$, as expected. For the RN dS exterior geometry with low values, this power-law tail appears quite clearly between the quasinormal zone and the exponential tail.

With such data, we can speak of three different regimes in the eld dynamics when one approaches the asymptotically flat limit. First, a quasinormal regime, with its characteristic damped oscillations, followed by an intermediate regime for which the power-law tail is visible and a late-time region for which an exponential tail dominates. This qualitative picture is valid for all elds considered.

VII. CONCLUSIONS

We have identified three regimes, according to the value of Λ for the decay of the scalar, electromagnetic and

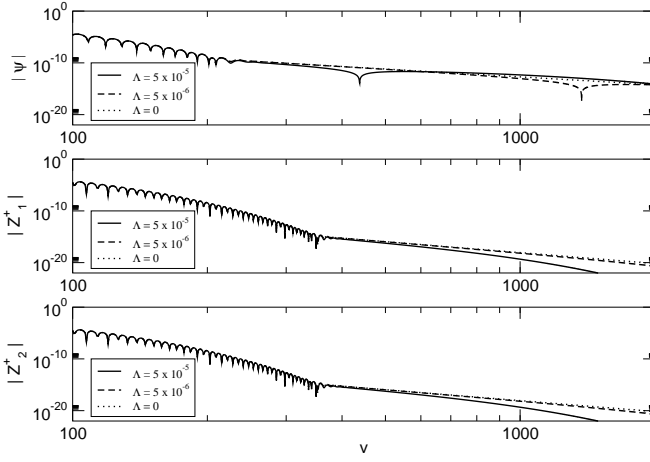


Figure 16: Scalar ($\ell = 1$), Z_1^+ and Z_2^+ fields ($\ell = 2$), approaching the asymptotically flat limit in RNds. The parameters for the geometry are $q = 0.5$ and $m = 1.0$. The results are similar for the other fields considered.

gravitational (or $Z_{1,2}$ in RNds) perturbations. Near the extreme limit (high ν), we have analytic expressions for the effective potentials and to the quasinormal frequencies. The decay is entirely dominated by the quasinormal modes (as in [31]), that is, oscillatory decaying characterized by a non-vanishing real part of the quasinormal frequency.

In an intermediary parameter region (lower ν), the wave functions have an important qualitative change, with the appearance of an exponential tail. This tail dominates the decay for large time. Near the asymptotically flat limit ($\nu \rightarrow 1$), we see an intermediary phase between the quasinormal modes and the exponential tail: a region of power-law decay. When $\nu = 0$, this region

entirely dominates the late-time behavior.

Finally, for scalar fields with $\ell = 0$ a constant decay mode appears, and its value depends on the $\psi(0; x)$ initial condition. Figure 6 reveals the appearance of the constant value ψ_0 for large t , and its dependence on $\psi(0; x)$. The value of ψ_0 falls below 10^{-7} for $\psi(0; x) = 0$. These results are compatible with the analytical predictions of [14]. The analytical characterization of these regions and the respective critical values of ν are crucial to a better understanding of these qualitatively different regimes.

A very important aspect of the field dynamics in the RNds geometries is that the influence of the electric charge on the field behavior, in general, was shown to be quite restricted. In particular we have observed no dependence of the exponential tail coefficients with q . This contrasts with previous results obtained in the anti-de Sitter case [8], where the charge plays a fundamental role in the tails. A deep understanding of this fact depends on new analytical asymptotic results in the lines of the ones obtained in [14]. These points are now under investigation. Also, since the presence of a charge implies an internal structure similar to that of a rotating black hole, our results might be interpreted as a broader universality of the frequencies here obtained. This question deserves further study.

Acknowledgments

This work was supported by Fundação de Amparo à Pesquisa do Estado de São Paulo (FAPESP), Conselho Nacional de Desenvolvimento Científico e Tecnológico (CNPq) and Coordenação de Aperfeiçoamento de Pessoal de Nível Superior (CAPES), Brazil.

-
- [1] T. Regge and J. A. Wheeler, *Phys. Rev.* **108**, 1063 (1957).
 - [2] S. Chandrasekhar, *The Mathematical Theory of Black Holes*, (Oxford University Press, Oxford, 1983).
 - [3] K. D. Kokkotas and B. G. Schmidt, *Living Rev. Relativity* **2** (1999).
 - [4] A. Riegg et al. *Astrophys. J.* **116**, 1009 (1998); S. Perlmutter et al., *Astrophys. J.* **517**, 565 (1999).
 - [5] V. Cardoso and J. P. S. Lemos, *Phys. Rev. D* **64**, 084017 (2001).
 - [6] B. Wang, C. Lin and E. Abdalla, *Phys. Lett. B*, **481**, 79 (2000); R. A. Konoplya, *Phys. Rev. D* **66**, 044009 (2002); E. Berti and K. D. Kokkotas, *Phys. Rev. D* **67**, 064020 (2003); V. Cardoso, R. Konoplya and J. P. S. Lemos, *Phys. Rev. D* **68**, 044024 (2003).
 - [7] V. Cardoso and J. P. S. Lemos, *Class. Quant. Grav.* **18**, 5257 (2001); V. Cardoso and J. P. S. Lemos, *Phys. Rev. D* **63**, 124015 (2001); J. M. Zhu, B. Wang and E. Abdalla, *Phys. Rev. D* **63**, 124004 (2001); B. Wang, E. Abdalla and R. B. Mann, *Phys. Rev. D* **65**, 084006. (2002).
 - [8] B. Wang, C. Molina and E. Abdalla, *Phys. Rev. D* **63**, 084001 (2001).
 - [9] H. Nariai, *Sci. Rep. Tohoku Univ.* **34**, 160 (1950); H. Nariai, *Sci. Rep. Tohoku Univ.* **35**, 62 (1951).
 - [10] E. W. Leaver, *Phys. Rev. D* **34**, 384 (1986).
 - [11] E. S. C. Ching, P. T. Leung, W. M. Suen and K. Young, *Phys. Rev. D* **52**, 2118 (1995).
 - [12] G. Gamow, *Zeits. F. Phys.* **51**, 204 (1928).
 - [13] P. R. Brady, C. M. Chambers, W. K. Ryan and P. Laguna, *Phys. Rev. D* **55**, 7538 (1997).
 - [14] P. R. Brady, C. M. Chambers, W. G. Laarakkers and E. Poisson, *Phys. Rev. D* **60**, 064003 (1999).
 - [15] B. F. Schutz and C. M. Will, *Astrophys. J.* **291**, L33 (1985).
 - [16] S. Iyer and C. M. Will, *Phys. Rev. D* **35**, 3621 (1987).
 - [17] S. Iyer, *Phys. Rev. D* **35**, 3632 (1987); K. D. Kokkotas and B. F. Schutz, *Phys. Rev. D* **37**, 3378 (1988).
 - [18] R. A. Konoplya, *Phys. Rev. D* **68**, 024018 (2003).
 - [19] A. Zhidenko, *Quasi-normal modes of Schwarzschild-de Sitter black holes*, gr-qc/0307012.
 - [20] S. Yoshida and T. Futamase, *Numerical analysis of quasinormal modes in nearly extremal Schwarzschild-de Sitter spacetimes*, gr-qc/0308077.

- [21] E. Abdalla, B. Wang, A. Lima-Santos and W. G. Qiu, Phys. Lett. B 538, 435 (2002); E. Abdalla, K. H. C. Castello-Branco, A. Lima-Santos, Mod. Phys. Lett. A 18, 1435 (2003).
- [22] R. Ruffini, J. Tiomno and C. Vishveshwara, Lettere al Nuovo Cimento 3, 211 (1972).
- [23] F. Mellor and I. Moss, Phys. Rev. D 41, 403 (1990).
- [24] C. Gundlach, R. Price and J. Pullin, Phys. Rev. D 49, 883 (1994).
- [25] R. Price, Phys. Rev. D 5, 2419 (1972).
- [26] A. R. Levander, Geophysics 53, 1425 (1988).
- [27] V. Cardoso and J. P. S. Lemos, Phys. Rev. D 67, 084020 (2003).
- [28] C. Molina, Phys. Rev. D 68, 064007 (2003).
- [29] G. Posch and E. Teller, Z. Phys. 83, 143 (1933).
- [30] V. Ferrari and B. Mashhoon, Phys. Rev. D 30, 295 (1984).
- [31] H. Beyer, Commun. Math. Phys. 204, 397 (1999).
- [32] H. Otsuki and T. Futamase, Prog. Theor. Phys. 85, 771 (1991); I. Moss and J. Norman, Class. Quant. Grav. 19, 2323 (2002).